The Silicon Vertex Detector of the Belle II Experiment

Y. Uematsu[q], K. Adamczyk[t], L. Aggarwal[i], H. Aihara[q], T. Aziz[j], S. Bacher[t], S. Bahinipati[f], G. Batignani[k,l], J. Baudot[e], P. K. Behera[g], S. Bettarini[k,l], T. Bilka[c], A. Bozek[t], F. Buchsteiner[b], G. Casarosa[k,l], L. Corona[k,l], T. Czank[p], S. B. Das[h], G. Dujany[e], C. Finck[e], F. Forti[k,l], M. Friedl[b], A. Gabrielli[m,n], E. Ganiev[m,n], B. Gobbo[n], S. Halder[j], K. Hara[r,o], S. Hazra[j], T. Higuchi[p], C. Irmler[b], A. Ishikawa[r,o], H. B. Jeon[s], Y. Jin[m,n], C. Joo[p], M. Kaleta[t], A. B. Kaliyar[j], J. Kandra[c], K. H. Kang[s], P. Kapusta[t], P. Kodyš[c], T. Kohriki[r], M. Kumar[h], R. Kumar[i], C. La Licata[p], K. Lalwani[h], R. Le Boucher[d], S. C. Lee[s], J. Libby[g], L. Martel[e], L. Massacesi[k,l], S. N. Mayekar[j], G. B. Mohanty[j], T. Morii[p], K. R. Nakamura[r,o], Z. Natkaniec[t], Y. Onuki[q], W. Ostrowicz[t], A. Paladino[k,l], E. Paoloni[k,l], H. Park[s], G. Polat[d], K. K. Rao[j], I. Ripp-Baudot[e], G. Rizzo[k,l], D. Sahoo[j], C. Schwanda[b], J. Serrano[d], J. Suzuki[r], S. Tanaka[r,o], H. Tanigawa[q], R. Thalmeier[b], R. Tiwari[j], T. Tsuboyama[r,o], O. Verbycka[t], L. Vitale[m,n], K. Wan[q], Z. Wang[q], J. Webb[a], J. Wiechczynski[l], H. Yin[b], L. Zani[d],

(Belle-II SVD Collaboration)

[a]School of Physics, University of Melbourne, Melbourne, Victoria 3010, Australia
[b]Institute of High Energy Physics, Austrian Academy of Sciences, 1050 Vienna, Austria
[c]Faculty of Mathematics and Physics, Charles University, 121 16 Prague, Czech Republic
[d]Aix Marseille Université , CNRS/IN2P3, CPPM, 13288 Marseille, France
[e]IPHC, UMR 7178, Université de Strasbourg, CNRS, 67037 Strasbourg, France
[f]Indian Institute of Technology Bhubaneswar, Satya Nagar, India
[g]Indian Institute of Technology Madras, Chennai 600036, India
[h]Malaviya National Institute of Technology Jaipur, Jaipur 302017, India
[i]Punjab Agricultural University, Ludhiana 141004, India
[j]Tata Institute of Fundamental Research, Mumbai 400005, India
[k]Dipartimento di Fisica, Università di Pisa, I-56127 Pisa, Italy
[l]INFN Sezione di Pisa, I-56127 Pisa, Italy
[m]Dipartimento di Fisica, Università di Trieste, I-34127 Trieste, Italy
[n]INFN Sezione di Trieste, I-34127 Trieste, Italy
[o]The Graduate University for Advanced Studies (SOKENDAI), Hayama 240-0193, Japan
[p]Kavli Institute for the Physics and Mathematics of the Universe (WPI), University of Tokyo, Kashiwa 277-8583, Japan
[q]Department of Physics, University of Tokyo, Tokyo 113-0033, Japan
[r]High Energy Accelerator Research Organization (KEK), Tsukuba 305-0801, Japan
[s]Department of Physics, Kyungpook National University, Daegu 41566, Korea
[t]H. Niewodniczanski Institute of Nuclear Physics, Krakow 31-342, Poland

Abstract

The Silicon Vertex Detector (SVD) is a part of the vertex detector in the Belle II experiment at the SuperKEKB collider (KEK, Japan). Since the start of data taking in spring 2019, the SVD has been operating stably and reliably with a high signal-to-noise ratio and hit efficiency, achieving good spatial resolution and high track reconstruction efficiency. The hit occupancy, which mostly comes from the beam-related background, is currently about 0.5% in the innermost layer, causing no impact on the SVD performance. In anticipation of the operation at higher luminosity in the next years, two strategies to sustain the tracking performance in future high beam background conditions have been developed and tested on data. One is to reduce the number of signal waveform samples to decrease dead time, data size, and occupancy. The other is to utilize the good hit-time resolution to reject the beam background hits. We also measured the radiation effects on the sensor current, strip noise, and full depletion voltage caused during the first two and a half years of operation. The results show no detrimental effect on the SVD performance.

Keywords: Silicon strip detector, Vertex detector, Tracking detector, Belle II

1. Introduction

The Belle II experiment [1] aims to probe new physics beyond the Standard Model in high-luminosity e^+e^- collisions at the SuperKEKB collider (KEK, Japan) [2]. SuperKEKB consists of the following components: injector LINAC, positron damping ring, and main storage ring with the electron and positron beamlines. The Belle II detector is located at the interaction point (IP) of the two beamlines. The main collision energy in the center-of-mass system is 10.58 GeV on the $\Upsilon(4S)$ resonance, which enables various physics programs based on the large samples of B mesons, τ leptons, and D mesons. Also, the asymmetric energy of the 7 GeV electron beam and 4 GeV positron beam is adopted for time-dependent CP violation measurements. The target of SuperKEKB is to accumulate an integrated luminosity of 50 ab^{-1} with peak luminosity of about

Email address: `uematsu@hep.phys.s.u-tokyo.ac.jp` (Y. Uematsu)

6×10^{35} cm^{-2}s^{-1}. In June 2021, SuperKEKB recorded the world's highest instantaneous luminosity of 3.1×10^{34} cm^{-2}s^{-1}. The data accumulated before July 2021 corresponds to an integrated luminosity of 213 fb^{-1}.

The Vertex Detector (VXD) is the innermost detector in the Belle II detector system. The VXD has six layers: the inner two layers (layers 1 and 2) are the Pixel Detector (PXD), and the outer four layers (layers 3 to 6) are the Silicon Vertex Detector (SVD). The schematic cross-sectional view of the VXD is shown in Fig. 1. The PXD consists of DEPFET pixel sensors, and its innermost radius is 1.4 cm from the IP. A detailed description of the SVD appears in Sec. 2.

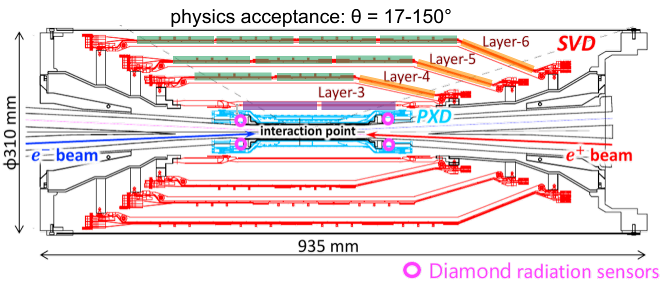

Figure 1: Schematic cross-sectional view of the VXD. The SVD is in red, the PXD is in light blue, and the IP beam pipe diamonds are in pink circles. In the upper half of the VXD the locations of the three types of SVD DSSDs are indicated by boxes in three colors: purple for small sensors, green for large sensors, and orange for trapezoidal sensors as described in Tab. 1.

Diamond sensors [3], used to monitor the radiation dose and for the beam abort system, are mounted on the IP beam pipe and the bellows pipes outside of the VXD. The pink circles in Fig. 1 indicate the locations of the diamond sensors on the IP beam pipe. The diamond's measured doses are used to estimate the dose in the SVD. The diamond system also sends beam abort requests to SuperKEKB if the radiation level gets too high to avoid severe damage to the detector.

2. Belle II Silicon Vertex Detector

The SVD is crucial for extrapolating the tracks to the PXD. This task is essential for measuring the decay vertices with the PXD and pointing at a region-of-interest limiting the PXD readout data volume. Other roles of the SVD are the standalone track reconstruction of low-momentum charged particles and their particle identification using ionization energy deposits. The SVD also plays a critical role in the decay vertex measurement in the case of long-lived particles like K_S mesons, which decay inside the SVD volume.

The SVD [4] consists of four layers of double-sided silicon strip detectors (DSSDs). The material budget of the SVD is about 0.7% of a radiation length per layer. On each DSSD plane, a local coordinate is defined with u and v: u-axis along n-side strips and v-axis perpendicular to u-axis. In other words, p-side strips and n-side strips provide u and v information, respectively. In the cylindrical coordinate, u corresponds to r–φ information and v corresponds to z information. The SVD consists of three types of sensors: "small" rectangular sensors in layer 3, "large" rectangular sensors in the barrel region of layers 4, 5, and 6, and "trapezoidal" sensors in the forward region of layers 4, 5, and 6, which is slanted. They are indicated by purple, green, and orange boxes in Fig. 1. The main characteristics of these three types of sensors are summarized in Tab. 1. The sensors are manufactured by two companies: the small and large sensors by Hamamatsu and trapezoidal sensors by Micron. The full depletion voltage is 60 V for Hamamatsu sensors and 20 V for Micron sensors; both types of sensors are operated at 100 V. In total, 172 sensors are assembled, corresponding to a total sensor area of 1.2 m^2 and approximately 224,000 readout strips.

	Small	Large	Trapezoidal
No. of u/p-strips	768	768	768
u/p-strip pitch	50 µm	75 µm	50–75 µm
No. of v/n-strips	768	512	512
v/n-strip pitch	160 µm	240 µm	240 µm
Thickness	320 µm	320 µm	300 µm
Manufacturer	Hamamatsu		Micron

Table 1: Table of the main characteristics of the three types of sensors. Only readout strips are taken into account for number of strips and strip pitch. All sensors have one intermediate floating strip between two readout strips.

Sensor strips are AC coupled to the front-end ASIC, the APV25 [5], which was originally developed for the CMS Silicon Tracker. The APV25 tolerates more than 100 Mrad of radiation. It has 128 channels with a shaping time of about 50 ns. For the SVD, the APV25 is operated in "multi-peak" mode. The mechanism of the data sampling in the multi-peak mode is explained in Fig. 2. The chip samples the height of the signal waveform with the 32 MHz clock (31 ns period) and stores each sample's information in an analog ring buffer. Since the bunch-crossing frequency is eight times faster than the sampling clock, the stored samples are not synchronous to the beam collision, in contrast to CMS, which motivates operation in the multi-peak mode. In the present readout configuration (the six-samples mode), at every reception of the Belle II global Level-1 trigger, the chip reads out six successive samples of the signal waveform stored in the buffers. The six-samples mode offers a wide enough time window (6×31 ns $= 187$ ns) to accommodate large timing shifts of the trigger. In preparation for operation with higher luminosity, where background occupancy, trigger dead-time, and the data size increase, we developed the three/six-mixed acquisition mode (mixed-mode). The mixed-mode is a new method to read out the signal samples from the APV25, in which the number of the samples changes between three and six in each event, depending on the timing precision of each Level-1 trigger signal in that event. For triggers with good timing precision, three-samples data are read out and the data have half time window and half data size compared to ones of six-samples data, resulting in the reduction of the effects due to higher luminosity. This functionality was already implemented in the running system and confirmed by a few hours of smooth physics data taking. Before we start to use the mixed-mode, the effect on the performance due to the change of the acquisition mode is to be assessed. As the first step, the effect in the hit efficiency was evaluated as described in Sec. 3.

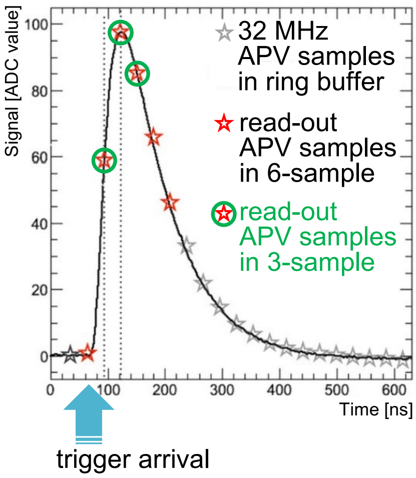

Figure 2: Example of sampling in "multi-peak" mode of the APV25. The black line shows the signal waveform after the CR-RC shaper circuit. The stars show the sampled signal height recorded in the analog ring buffer according to the 32 MHz sampling clock. The red stars indicate the six successive samples read out at the trigger reception in the six-samples mode. The red stars with a green circle indicate the samples read out in the three-samples acquisition.

The APV25 chips are mounted on each middle sensor (chip-on-sensor concept) with thermal isolation foam in between. The merit of this concept is shorter signal propagation length, leading to smaller capacitance of the signal line and hence reduced noise level. To minimize the material budget the APV25 chips on the sensor are thinned down to 100 μm. The APV25 chips are mounted on a single side of the sensor and readout of the signals from the opposite side is performed via wrapped flexible printed circuits. The power consumption of the APV25 chip is 0.4 W/chip and in total 700 W in the entire SVD. The chips are cooled by a bi-phase –20°C CO_2 evaporative cooling system.

3. Performance

The SVD was combined with the PXD to complete the VXD assembly in October 2018, and the VXD was installed to the Belle II detector system in November 2018. Since March 2019, the SVD has been operating reliably and smoothly for two and a half years. The total fraction of masked strips is about 1%. There was only one issue where one APV25 chip (out of 1,748 chips) was disabled during the spring of 2019, which was remediated by reconnecting a cable in the summer of 2019.

The SVD has also demonstrated stable and excellent performance [6]. The hit efficiency is continuously over 99% in most of the sensors. The cluster charge distributions are also reasonable. On the u/p-side, the most probable values agree with the calculated charge amount induced by MIPs within the uncertainty in calibration. On the v/n-side, 10–30% of the collected charge is lost compared to the signal collected on the u/p-side, due to the presence of the floating strip combined with the large pitch on the v/n-side. The most probable values of the cluster signal-to-noise ratio distributions range from 13 to 30.

We measured the cluster position resolution by analyzing the $e^+e^- \to \mu^+\mu^-$ data [7]. The cluster position resolution is estimated from the residual between the cluster position and the track position, not biased by the target cluster, after subtracting the effect of the track extrapolation error. The cluster position resolutions for different incident angles are shown in Fig. 3. The observed resolution has the expected shape, showing a minimum at the incident angle for which the projection of the track along the direction perpendicular to the strips on the detector plane corresponds to two strip pitches. Given the various sensor pitches with one floating strip, the minimum is expected at 14 (21) degrees on the v/n-side and at 4 (7) degrees on the u/p-side, respectively for layer 3 (4, 5, and 6). The resolution for normal incident angle is also in good agreement with the expected digital resolution, that is 23 (35) μm on the v/n-side, 7 (11) μm on the u/p-side, respectively for layer 3 (4, 5, and 6). Still, some studies are ongoing to improve the analysis for the cluster resolution especially for the layer-3 u/p-side, where at normal incidence a slightly higher resolution is measured (9 μm) compared to the expectations .

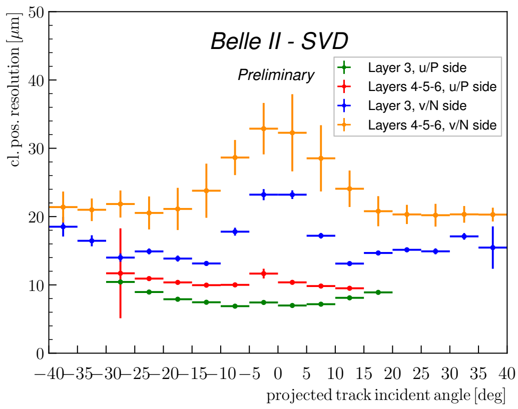

Figure 3: The SVD cluster position resolution depending on the projected track incident angle. The green (blue) plot shows the resolution in the u/p-side (n/v-side) of layer-3 sensors, and the red (yellow) one shows the u/p-side (n/v-side) of layers-4, 5, and 6 sensors.

The cluster hit-time resolution was also evaluated in candidate hadronic events[1] using the reference event time estimated by the Central Drift Chamber (CDC) outside of the SVD. The error on the event time, about 0.7 ns, was subtracted to evaluate the intrinsic SVD hit-time resolution. The resulting resolution is 2.9 ns on the u/p-side and 2.4 ns on the v/n-side. With such precise hit-time information, it is possible to reject off-time background hits efficiently. The hit-time distributions for signal[2] and background[3] are shown in Fig. 4. The signal distribution has a narrow peak, while the background hit-time distribution is broad and almost flat in the signal peak region. The

[1] The events with more than three good tracks and not like Bhabha scattering.
[2] The clusters found to be used in the tracks in the hadronic events.
[3] The clusters in events triggered by delayed-Bhabha pseudo-random trigger.

separation power of the hit-time is high, as expected. For example, if we reject hits with the hit-time less than −38 ns in this plot, we can reject 45% of the background hits while keeping 99% of the signal hits. The background rejection based on the hit-time is essential to sustain the good tracking performance in the future high beam background condition.

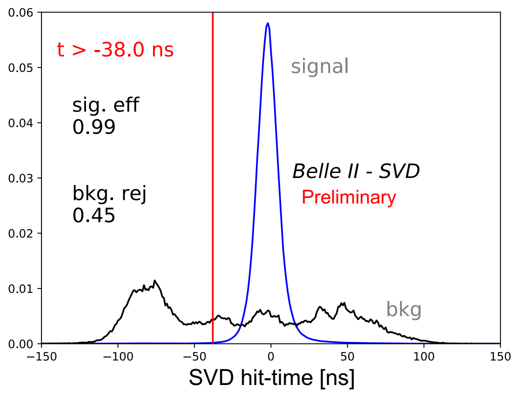

Figure 4: Example of the background hit rejection using hit-time. The blue distribution shows the signal, and the black distribution shows the background. Assuming the hit-time cut at −38 ns, the signal hit efficiency of 99% and the background hit rejection of 45% are achieved.

The performance in three-samples data was compared with that in six-samples data to evaluate the performance in the mixed-mode. If the trigger timing has no deviation, the three-samples data will show comparable performance to the six-samples data because the relevant part of the signal waveform to evaluate the necessary signal properties, i.e., the signal height and the signal timing, can be accommodated in the three-sample's time window. However, when the trigger has a jitter and the timing shift happens, some part of the signal waveform can be out of the three-sample's time window, and the reconstruction performance deteriorates. We examined the effect on the hit efficiency as a function of the trigger timing shift. The effect is evaluated by the relative hit efficiency, which is defined as the ratio of the hit efficiency in the three-samples data to the one in the six-samples data. For this study, the three-samples data are emulated in the offline analysis from the six-samples data by selecting consecutive three samples at a fixed latency with respect to the Level-1 trigger signal. The trigger timing shift is evaluated by the CDC event time. The resulting relative efficiencies as a function of the trigger timing shift in the hadronic events are shown in Fig. 5. The decreasing trend is observed for the shift of the trigger timing, as expected. As a result, the relative efficiency is over 99.9% for the trigger timing shift within ±30 ns, which is almost all the events.

4. Beam-related background effects on SVD

The beam-related background increases the hit occupancy of the SVD, which in turn degrades the tracking performance. Considering this performance degradation, we set the occupancy limit in layer-3 sensors to be about 3%, which will be

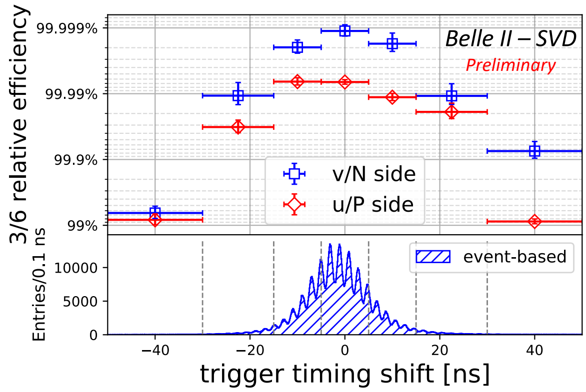

Figure 5: The relative hit efficiencies (the ratios of the hit efficiency in the three-samples data to the one in the six-samples data) as a function of the trigger timing shift for v/n-side (blue square) and u/p-side (red diamond). The positive (negative) trigger timing shift corresponds to early (late) trigger timing.

loosened roughly by a factor of two after we apply the hit-time rejection described in Sec. 3. With the current luminosity, the average hit occupancy in layer-3 sensors is less than 0.5%. However, the projection of the hit occupancy at the luminosity of 8×10^{35} cm^{-2}s^{-1} is about 3% in layer-3 sensors. The projected occupancy comes from the Monte Carlo (MC) simulation scaled by the data/MC ratio determined from the beam background data of the current beam optics. The corresponding integrated dose, using the data/MC-rescaled beam background extrapolation, is about 0.2 Mrad/smy, and the equivalent 1-MeV neutron fluence is about 5×10^{11} n_{eq}/cm^2/smy (smy: Snowmass Year = 10^7 sec). Considering the radiation hardness of the SVD sensors, about 10 Mrad and about 10^{13} n_{eq}/cm^2, based on the experience of similar DSSD sensors used in the BaBar Silicon Vertex Tracker [8], we expect to be able to safely operate the SVD even for ten years at high luminosity, with some safety margin with respect to beam background extrapolation of about a factor two to three. The long-term extrapolation of the beam background is affected by large uncertainties from the optimization of collimator settings in MC and the future evolution of the beam injection background, which is not simulated. This uncertainty, together with the relatively small safety factor two to three between the beam background extrapolation and the detector limits, motivates the VXD upgrade which improves the tolerance of the hit rates and the radiation damage, and the technology assessment is ongoing for multiple sensor options.

In the first two and a half years of operation the integrated radiation dose in the layer-3 mid-plane sensors, which are the most exposed in the SVD, is estimated to be 70 krad. The estimation is based on the measured dose by the diamonds on the beam pipe exploiting the measured correlation between the SVD occupancy and the diamond dose [9]. Thanks to the introduction of a new random trigger line, recently made available, we could improve the dose analysis, removing a bias of about a factor 3 that gave an overestimation of the dose in the previous analysis. The new estimate still has an uncertainty of about 50%, mainly due to the unavailability of the appropriate trigger before December 2020. Assuming the dose/n_{eq} fluence ratio of

2.3×10^9 n_{eq}/cm^2/krad from MC, 1-MeV equivalent neutron fluence is evaluated to be about 1.6×10^{11} n_{eq}/cm^2 in the first two and a half years.

The effect of the integrated dose on the sensor leakage current is measured, and the results show a clear linear correlation as in the upper plot of Fig. 6. The slopes for all the sensors are 2–5 $\mu A/cm^2$/Mrad, as summarized in the lower plot of Fig. 6. The large variations can be explained by temperature effects and the deviation of sensor-by-sensor dose from the average in each layer used in the estimation. The slopes are in the same order of magnitude as previously measured in the BaBar experiment [8], 1 $\mu A/cm^2$/Mrad at 20°C. The precise temperature in layer 3 of the SVD is unknown, but expected to be in a similar regime. While the leakage current is increasing, the impact on the strip noise is suppressed by the short shaping time (50 ns) in APV25. It is expected to be comparable to the strip-capacitive noise only after 10 Mrad irradiation and not problematic for ten years where the integrated dose is estimated to be 2 Mrad.

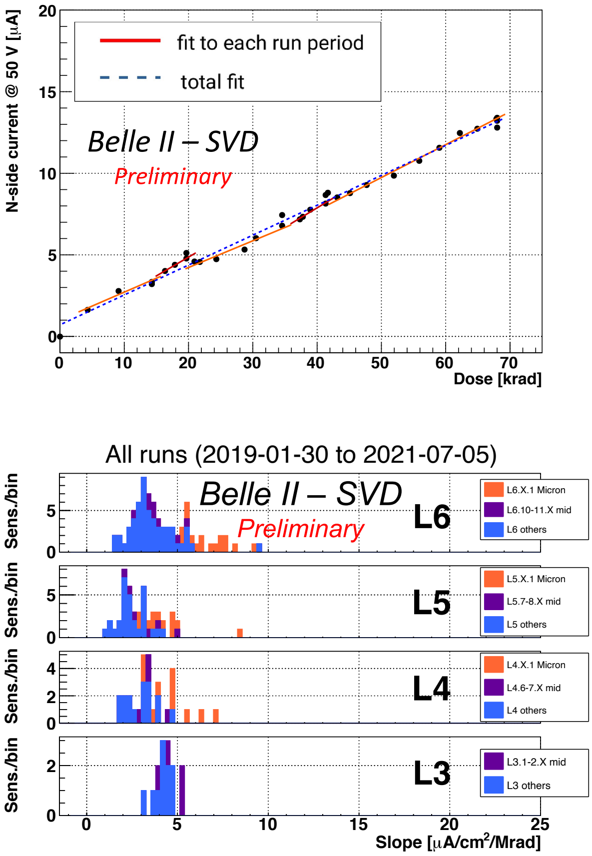

Figure 6: (upper) Effect of the integrated dose on the leakage current in the n/v-side of one layer-3 sensor. The slope is fitted for each run period (solid red line) and all the runs (dashed blue line). Both fit results agree with each other and are consistent with the linear increase. (lower) The fit results of all the sensors for all runs. The sensors are classified as trapezoidal sensors in the forward region (Micron), sensors around the midplane, and the others.

The evolution of the noise with the integrated dose is shown in Fig. 7. The noise increase of 20–25% is observed in layer 3, but this does not affect the SVD performance. This noise increase is likely due to the radiation effects on the sensor surface. Fixed oxide charges on sensor surface increase with dose, with some saturation expected at around 100 krad, enlarging also non-linearly the inter-strip capacitance, also expected to saturate with dose. The noise saturation is already observed on the v/n-side and also starts to be seen on the u/p-side.

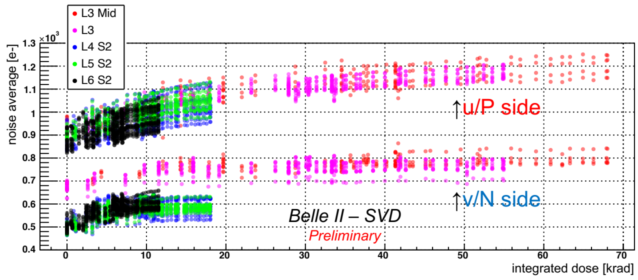

Figure 7: Effect of the integrated dose on the noise average in electron. The clear increase is observed and saturated (or start to be saturated) for layer-3 sensors.

The full depletion voltage of the sensor is also a key property that can be affected by the radiation damage. It can be measured from the v/n-side strip noise, which suddenly decreases at the full depletion voltage because the sensor substrate is n-type and thus the v/n-side strips are only fully isolated at full depletion. From this measurement full depletion voltages consistent with measurements performed on the bare sensors before the installation were obtained, ranging from 20 to 60 V, and so far no change in full depletion voltage is observed in the first two and a half years of operation, which is consistent with the expectation from low integrated neutron fluence of 1.6×10^{11} n_{eq}/cm^2.

5. Conclusions

The SVD has been taking data in Belle II since March 2019 smoothly and reliably. The detector performance is excellent and agrees with expectations. We are ready to cope with the increased background during higher luminosity running by rejecting the off-time background hits using hit-time and operating in the three/six-mixed acquisition mode. In the recent study, the efficiency loss in the three-samples data is confirmed to be less than 0.1% for the trigger timing shift within ±30 ns. The observed first effects of radiation damage are also within expectation and do not affect the detector performance.

Acknowledgments

This project has received funding from the European Union's Horizon 2020 research and innovation programme under the Marie Sklodowska-Curie grant agreements No 644294 and 822070. This work is supported by MEXT, WPI, and JSPS (Japan); ARC (Australia); BMBWF (Austria); MSMT (Czechia); CNRS/IN2P3 (France); AIDA-2020 (Germany); DAE and DST (India); INFN (Italy); NRF and RSRI (Korea); and MNiSW (Poland).

References

[1] T. Abe, et al., Belle II Technical Design Report (2010). arXiv:1011.0352.

[2] Y. Ohnishi, et al., Accelerator design at SuperKEKB, Prog. Theor. Exp. Phys. 2013 (3), 03A011 (03 2013).

[3] S. Bacher, et al., Performance of the diamond-based beam-loss monitor system of Belle II, Nucl. Instrum. Methods Phys. Res., Sect. A 997 (2021) 165157. arXiv:2102.04800.

[4] K. Adamczyk, et al., The Belle II silicon vertex detector assembly and mechanics, Nucl. Instrum. Methods Phys. Res., Sect. A 845 (2017) 38–42, proceedings of the Vienna Conference on Instrumentation 2016.

[5] M. J. French, et al., Design and results from the APV25, a deep sub-micron CMOS front-end chip for the CMS tracker, Nucl. Instrum. Methods Phys. Res., Sect. A 466 (2001) 359–365.

[6] G. Rizzo, et al., The Belle II Silicon Vertex Detector: Performance and Operational Experience in the First Year of Data Taking, JPS Conf. Proc. 34, 010003 (2021).

[7] R. L. Boucher, et al., Measurement of the cluster position resolution of the Belle II Silicon Vertex Detector, these NIMA Conference Proceedings.

[8] B. Aubert, et al., The BaBar detector: Upgrades, operation and performance, Nucl. Instrum. Methods Phys. Res., Sect. A 729 (2013) 615–701.

[9] L. Massaccesi, Performance study of the SVD detector of Belle II and future upgrades, master thesis, Departomento di Fisica *E. Fermi*, Università di Pisa (2021).
URL `https://docs.belle2.org/record/2759/`